applied sciences

MDPI

Article

Quantifying Privacy Risks for Continuous Trait Data

Muqing He [1], Deqing Zou [1,*], Weizhong Qiang [1], Shouhuai Xu [2], Wenbo Wu [3] and Hai Jin [4]

[1] National Engineering Research Center for Big Data Technology and System, Services Computing Technology and System Lab, Hubei Key Laboratory of Distributed System Security, Hubei Engineering Research Center on Big Data Security, School of Cyber Science and Engineering, Huazhong University of Science and Technology, Wuhan 430074, China

[2] College of Engineering and Applied Science, University of Colorado at Colorado Springs, Colorado Springs, CO 80918, USA

[3] College of Business, The University of Texas at San Antonio, San Antonio, TX 78249, USA

[4] National Engineering Research Center for Big Data Technology and System, Services Computing Technology and System Lab, Cluster and Grid Computing Lab, School of Computer Science and Technology, Huazhong University of Science and Technology, Wuhan 430074, China

* Correspondence: deqingzou@hust.edu.cn

Abstract: In the context of life sciences, the rapid biotechnical development leads to the creation of huge amounts of biological data. The use of such data naturally brings concerns on human genetic privacy breaches, which also discourage biological data sharing. Prior studies have investigated the possibility of the privacy issues associated with individuals' trait data. However, there are few studies on quantitatively analyzing the probability of the privacy risk. In this paper, we fill this void by proposing a scheme for systematically breaching genomic privacy, which is centered on quantifying the probability of the privacy risk of continuous trait data. With well-designed synthetic datasets, our theoretical analysis and experiments lead to several important findings, such as: (i) The size of genetic signatures and the *sensitivity* (true positive rate) significantly affect the accuracy of re-identification attack. (ii) Both the size of genetic signatures and the minor allele frequency have a significant impact on distinguishing true positive and false positive matching between traits and genetic profiles. (iii) The size of the matching quantitative trait locus dataset has a large impact on the confidence of the privacy risk assessment. Validation with a real dataset shows that our findings can effectively estimate the privacy risks of the continuous trait dataset.

Keywords: genomic privacy; re-identification; quantitative trait locus; sensitivity

check for updates

Citation: He, M.; Zou, D.; Qiang, W.; Xu, S.; Wu, W.; Jin, H. Quantifying Privacy Risks for Continuous Trait Data. *Appl. Sci.* **2022**, *12*, 10586. https://doi.org/10.3390/app122010586

Academic Editor: David Megías

Received: 20 September 2022
Accepted: 17 October 2022
Published: 20 October 2022

1. Introduction

Since the HapMap Project [1], genome sequencing has undergone considerable development with advancements that can greatly reduce the time and material expenses of DNA profiling that promote the development of bioinformatics [2–4]. Quantitative Trait Loci (QTL) [5], which is based on bioinformatics, is now a proven technique for large-scale biodata analysis [6] and is not only conducted in academic research but also widely commercialized as supporting services for direct-to-consumer DNA testing [7,8]. For example, QTL analysis revealed the presence of genetic mutations highly associated with cancer incidence [9–11].

While the resulting large amounts of data can facilitate revolutionary advancements in medical science and healthcare [12], the risk of genomic privacy breach has become an important concern, which arises when using and sharing genomic data because such data contains a series of information related to personal and familial privacy [13]. A unique threat posed by genomic data is that an individual's genomic information not only breaches the privacy of the individual in question but also exposes a substantial amount of information about the individual's relatives [14,15]. Combining with reidentification privacy risks by matching anonymized medical data with public genomic data [16,17], genomic privacy breaches will have long-term adverse effects on individuals and their families.

For the reasons above, both the executive branch and academia have paid increasing attention to genomic privacy. The US health care system has established strict privacy rules for the usage of genomic data [18], while the community website GenomePrivacy.org integrate genome privacy and security information for academic studies [19]. On the other hand, academic research has identified genomic privacy breaches or reidentification risks [20–22]. Specifically, Schadt et al. [20] used the top 1000 *cis* eQTLs for reidentification on an expression database from the entire US population and achieved a Type 1 error of 10^{-5} (wrongly identifying an innocent individual as a victim) and an accuracy of 85%. Backes et al. [21] achieved a reidentification accuracy of 97.5% by relating DNA methylation data with genomic methylation Single Nucleotide Polymorphism (SNP) data. Sero et al. [22] designed face-to-DNA classifiers to associate face images and genomic data, demonstrating substantial true matching (training accuracy 83%, verification accuracy 80%).

However, previous studies only focus on qualitatively analyzing whether potential re-identification risks exist, but few studies have quantitatively analyzed under what circumstances re-identification risks exist. Eric E Schadt et al. [20], Lippert et al. [23], and Michael Backes et al. [21] focused on the possibility of privacy threat between DNA and phenotypes; all of their quantitative analyses were intended to illustrate the existence of the privacy threat, with little mention of how serious the privacy risks was in different situations. Furthermore, all the previous studies are limited to a certain class of continuous trait data. Lippert et al. [23] limited their quantitative models for just a few common phenotypes, Eric E Schadt et al. [20] only verified the privacy risks of RNA expression data, Michael Backes et al. [21] only estimated identification risks of methylation data with small overlap between distributions. In general, previous works had not proposed a method to predict the privacy risk of any set of continuous traits.

Contributions. In this paper, we provide the first detailed quantitative derivation for the probability of the privacy risks of continuous trait data, which can be used to measure the vulnerability, the probability that the data will be unable to resist the privacy-breaching attack [24]. Our contributions can be divided into three major areas. (i) We formalize the genome privacy breaching attack as a series of single-feature three-classification problems. This formalization also allows us to construct synthetic data with configurable parameters, which is needed because our quantitative analysis requires parameters that can be set. Moreover, there are few real-world data for testing our approaches. (ii) We present a Bayesian method that matches continuous trait profiles to the genotypes. This allows us to draw deeper insights, such as: the factor affecting the matching accuracy does not depend on the *accuracy* of classification but depends on the *sensitivity* (see Section 6.3.1) and the number of continuous traits; both the prior probabilities of genotypes and the number of continuous traits have significant impacts on distinguishing true positive and false positive matching; the larger the matching dataset, the lower the privacy risk. (iii) Our analysis of the real dataset confirms that with *sensitivity*, the number of traits, and the prior probabilities of genotypes, we can accurately estimate the privacy implications of a trait dataset.

Organization. We introduce the background knowledge about traits and genotypes in Section 2, review the relevant previous work in Section 3, present our adversarial model in Section 4, and then describe the principle of synthetic data generation in Section 5. In Section 6, we analyze the main factors affecting data privacy risk through simulation experiments and mathematical derivation and verified our analysis results with real data. We also discuss the application scenarios of our findings and what needs to be improved in future work in Section 7, before concluding in Section 8.

2. Preliminaries

In this section, we review three biological concepts that are used throughout the paper. The concept of SNP is used for describing the differences between individual genes. The concept of QTL describes the association between epigenetic characteristics and genes. The concept of MAF reflects the prior probability of different genes.

2.1. SNP (Single Nucleotide Polymorphism)

SNP is an important concept in the context of the present paper because it can be exploited for genomic privacy breaching. This is possible because SNP is the most common and representative heritable genetic variant. An SNP is the variation of a single nucleotide in DNA; this variation can be a transition (e.g., Cytosine to Thymine) or transversion (e.g., Cytosine to Adenine) of a single nucleotide. SNPs are effectively the digenic type in most cases [25]; each SNP usually contains two alleles, called major and minor alleles, respectively. Studies show that there are strong correlations between SNPs and some specific diseases, such as the incidence of Alzheimer's disease, which is highly correlated with particular SNPs [26]. This means that for genomic privacy breaching or reidentification purposes, an attacker does not need to use the entire DNA sequence; rather, the attacker only needs to consider DNA variations, which can be effectively measured via SNPs.

2.2. QTL (Quantitative Trait Loci)

A QTL is a region of the genome that is associated with a particular phenotypic trait, which can be attributed to a polygenic effect [27]. At a high level, the QTLs that are located near their original genes are known as *cis* QTLs, whereas the ones that are located far from their original genes are known as *trans* QTLs. To reduce the impact that the sample sizes of many QTL studies are small [28], researchers have combined QTLs and global gene expression for mapping the genetic features to expressions from numerous transcripts [29].

2.3. MAF (Minor Allele Frequency)

The MAF is the prior probabilities of SNPs' rare variants from a given population [30,31]. A digenic SNP can be considered as a combination of independent DNA bases A and B with occurrence probability $\Pr(A)$ and $\Pr(B)$ such that $\Pr(A) + \Pr(B) = 1$. Then the MAF is the minor value of $\Pr(A)$ and $\Pr(B)$. Let AA denote the case or event where SNP takes the value (A, A), BB denote the case where SNP takes the value (B, B), and AB denote the case where SNP takes the value (A, B) or (B, A). We have $\Pr(AA) = \Pr(A)^2$, $\Pr(BB) = \Pr(B)^2$, and $\Pr(AB) = 2\Pr(A)\Pr(B)$ as A and B are independent.

3. Related Work

In the context of the present paper, genomic privacy risk can be mainly divided into several scenarios, such as the $n = 1$ *scenario*, the *summary statistic scenario*, and the *gene expression scenario*, etc.

Studies in the $n = 1$ **scenario**. In this scenario, the sensitive traits are correlated with individual's genotype directly [32]. Several attacks have been proposed for this scenario. Pakstis et al. [33] discovered that approximately 45 carefully chosen SNPs could be used for major global population identification with a *type* 1 *error* of 10^{-15}. More generally, Zhen Lin et al. [34] summarized the influence of matching accuracy with the average MAF, number of SNPs and population, measured the TPR and FPR of predicitons correlated to these parameters in the $n = 1$ *scenario*, and revealed that a random subset of approximately 300 SNPs with an MAF $\leqslant 0.1$ was sufficient to uniquely identify any person around the world. A more recent study on Beacon [35] demonstrate that only 1000 "yes or no" queries for SNPs can detect the presence of an individual from the Personal Genome Project [36]. To against this situation, in a study on methylation data sharing in Beacon, Inken Hagestedt et al. [37] proposed the MBeacon system for private DNA methylation data sharing with a comparison test.

Studies in the summary statistic scenario. In this scenarios, Compared with the allele frequencies of the general population, allele frequencies from the case group will be positively biased toward the target genotypes [32], which was investigated in a landmark study by Nils Homer et al. [38], who found that ADAD on GWAS data could be achieved only with the study participants' allele frequencies. Subsequent researches expanded the scope of the vulnerabilities for summary statistics and analysed its mathematical properties [39–41].

Studies in the gene expression scenario. In this scenarios, gene expressions that are linked to a series of attributes, such as QTL data, could be used for genomic privacy breaching. As Eric E Schadt et al. mentioned [20], with a training step using a standard reference eQTL data set, a Bayesian approach could be used to calculate the probability distributions of the expression data with given genotypes. The researchers then matched the target genotype and tested the TPR and FPR of this matching. with the top 1000 *cis* eQTLs, this ADAD technique had high accuracy in large-scale simulations. Robert A Philibert et al. [42] notably emphasized this scenario with specific methylation data. Stephanie O. M. Dyke et al. [43] described the biomolecular mechanism by which methylation data could lead to a privacy risk by analysing real data. Subsequently, Michael Backes et al. [21] used the Bayesian method adapted from As Eric E Schadt's work [20] to correlate the methylation profile to an individual genotype, which had an up to 97.5% matching accuracy with 293 independent meQTL-methylation pairs and without false positive predictions on a dataset of nearly 3000 samples. They also proved that the continuous distribution function could be best fixed as a normal distribution, which supports the findings of our simulation experiments. Lippert et al. [23] used 1062 volunteer samples for analysis and found that the associations between some common phenotypes and genes could lead to privacy threats. The findings of a more resent study from Dzemila Sero et al. [22], who used high-resolution 3D facial data and correlated them with SNP profiles, was challenged by Rajagopal Venkatesaramani et al. [44] in terms of the actual feasibility.

Studies in the other scenarios. Regarding genomic privacy breaches, several papers have studied privacy risks related to various sorts of additional data or in spatial conditions with large-scale spatio-temporal extents. Gymrek et al. showed that genotypes can be reidentified with genetic traits on the Y chromosome by querying genetic genealogy databases [45]. Humbert et al. showed that SNPs can also be exploited to further reidentify anonymous genotypes by typically using side channels [14]. Backes et al. proposed a model for quantifying the impact of the continuous sequencing and publicizing of personal genomic data on a population's genomic privacy [46], which demonstrated that an increasing sharing rate in the future will entail a substantial negative effect on the privacy of all older generations. Berrang et al. presented a generic framework for quantifying the privacy risks in biomedical data taking into account the various interdependencies between data of different types, from different individuals, and at different times [47]. With this framework, an adversary can efficiently identify the parent-child relationships based on methylation data with a success rate of 95%.

4. Model and Methodology

To characterize the privacy risks of anonymous continuous trait data without protection, we propose a privacy-breaching attack method that can reveal sensitive personal information based on a calculated approach while leveraging publicly available data. In this section, we first introduce adversarial models for privacy breaching and then introduce our attack methods.

4.1. Threat Model

We consider a scenario where the adversary has access to both genetic data and continuous trait data. The continuous trait data is anonymous, while some shareable genetic profiles have real identifiers, such as information that can be targeted to specific individuals. Examples of genetic databases include OpenSNP [16] and the Personal Genome Project [17]. This information can be taken by the adversary to re-identify personal information from other anonymous continuous trait data [48]. Furthermore, even if a genetic profile is anonymous, the adversary can still link it to its pedigree with surname-genome associations [45], kinships [14], or online social networks [49].

We assume a threat model under which the correlations between continuous traits and SNPs may be acquired as the background knowledge by the adversary, as shown in Figure 1. First, there are two ways for an adversary to obtain this background knowledge. One approach is to obtain the relationships by analyzing public QTL datasets, such as the cerebrospinal fluid proteome dataset in National Center for Biotechnology Information (NCBI) [48]. The other approach is to rely on existing findings of the statistical relationships between genes and continuous traits. For example, the adversary can obtain prior probabilities, expectations, and standard deviations of RNA-binding proteins (RBP) with disease-related SNPs from academic QTLs websites [50]. Next, the adversary needs to determine whether the individual genomic profile is the member of the continuous trait dataset, and if so, which individual. Finally, the adversary successfully matches continuous trait profile and genotype as the same individual, which leads to privacy breaches.

4.2. Attack Methodology

The continuous trait data and SNP data can be presented as a $m_t \times n_t$ array $\mathbb{T}$ and a $m_s \times n_s$ array $\mathbb{S}$, respectively. The k-th column in $\mathbb{T}$, denoted by $\mathbb{T}(\cdot, k)$, contains individual k's all continuous traits, and the i-th row in $\mathbb{T}$, denoted by $\mathbb{T}(i, \cdot)$ contains i-th continuous trait for all individuals. Similarly, $\mathbb{S}(\cdot, l)$ and $\mathbb{S}(j, \cdot)$ represent the individual l's genomic profile and j-th SNP for all individuals respectively. In general, the number of the genetic loci is much larger than the number of continuous traits (i.e., $j \gg i$). It has been shown that there are multiple $\mathbb{S}(j, \cdot)$ corresponding to one $\mathbb{T}(i, \cdot)$ as QTLs in the vast majority of cases [48]. Let $\Omega(i)$ be an index set for the SNPs that are correlated with the i-th continuous trait. Then $\mathbb{S}(\Omega(i), l)$ contains the values of SNPs that are correlated with the i-th continuous trait for individual l.

The deanonymization attack contains two stages. In the first stage, the adversary obtains the prior probabilities, expectations, and standard deviations as the correlations between $\mathbb{S}(\Omega(i), \cdot)$ and $\mathbb{T}(i, \cdot)$. In the next stage, based on this knowledge, the adversary is able to identify the best-matched pair $\{\mathbb{S}(\cdot, l^*), \mathbb{T}(\cdot, k^*)\}$ and determine whether the SNP profile $\mathbb{S}(\cdot, l^*)$ and continuous trait profile $\mathbb{T}(\cdot, k^*)$ belong to the same person.

As mentioned in Section 4.1, There are two approaches for the adversary to acquire correlations between SNPs and continuous traits. For the second approach, the adversary can obtain the prior probabilities, expectations, and standard deviations directly; for the first approach, the probabilistic relationships between the continuous traits and genetic loci are derived through training data which are either publicly available or the adversary has access to, and is the focal point of this subsection. Note that the members of the continuous trait data correspond one-to-one with the members of the SNP data in the training set, for example, $\mathbb{T}(\cdot, k)$ and $\mathbb{S}(\cdot, k)$ are from the same individual. In addition, for the training set, each SNP in corresponding to $\mathbb{S}(j, \cdot)$ is corresponding to at least one continuous trait in $\mathbb{T}(i, \cdot)$, while each continuous trait in $\mathbb{T}(i, \cdot)$ has at least one corresponding SNP in $\mathbb{S}(j, \cdot)$.

It should be noted that our approach is related to the works of Michael Backes et al. [21] and Eric E Schadt et al. [20]. However, these two studies limited their traits to certain types (methylation level and *cis* RNA level), while our approach adopts continuous traits that are more general. Furthermore, different from these two studies which approximately used normal distribution to estimate the probabilities of the continuous trait values at different genotypes, since most of the continuous trait values are greater than zero, we adopt a truncated normal distribution for $\Pr(\mathbb{S}(j, l) | \mathbb{T}(i, k))$ estimation that is more realistic. We will describe this approach in greater detail.

Let T_i be a continuous random variable that measures the value of the i-th quantitative measure and let $S_{\Omega(i)}$ be the region of SNPs that are mostly correlated to T_i. The goal is to obtain the posterior probability for $S_{\Omega(i)}$ to take value $\mathbb{S}(\Omega(i), k)$ for an individual person k if T_i takes value $\mathbb{T}(i, k)$ for the same person, that is, to obtain $\Pr\left(S_{\Omega(i)} = \mathbb{S}(\Omega(i), k) | T_i = \mathbb{T}(i, k)\right)$ for any k. By the Bayes rule, we have

$$\begin{aligned}&\Pr\left(S_{\Omega(i)} = \mathbb{S}(\Omega(i),k) | T_i = \mathbb{T}(i,k)\right) \\ &= \frac{\Pr\left(T_i = \mathbb{T}(i,k) | S_{\Omega(i)} = \mathbb{S}(\Omega(i),k)\right) \Pr\left(S_{\Omega(i)} = \mathbb{S}(\Omega(i),k)\right)}{\sum_{i=1}^{m} \Pr\left(T_i = \mathbb{T}(i,k) | S_{\Omega(i)} = \mathbb{S}(\Omega(i),k)\right) \Pr\left(S_{\Omega(i)} = \mathbb{S}(\Omega(i),k)\right)}\end{aligned} \tag{1}$$

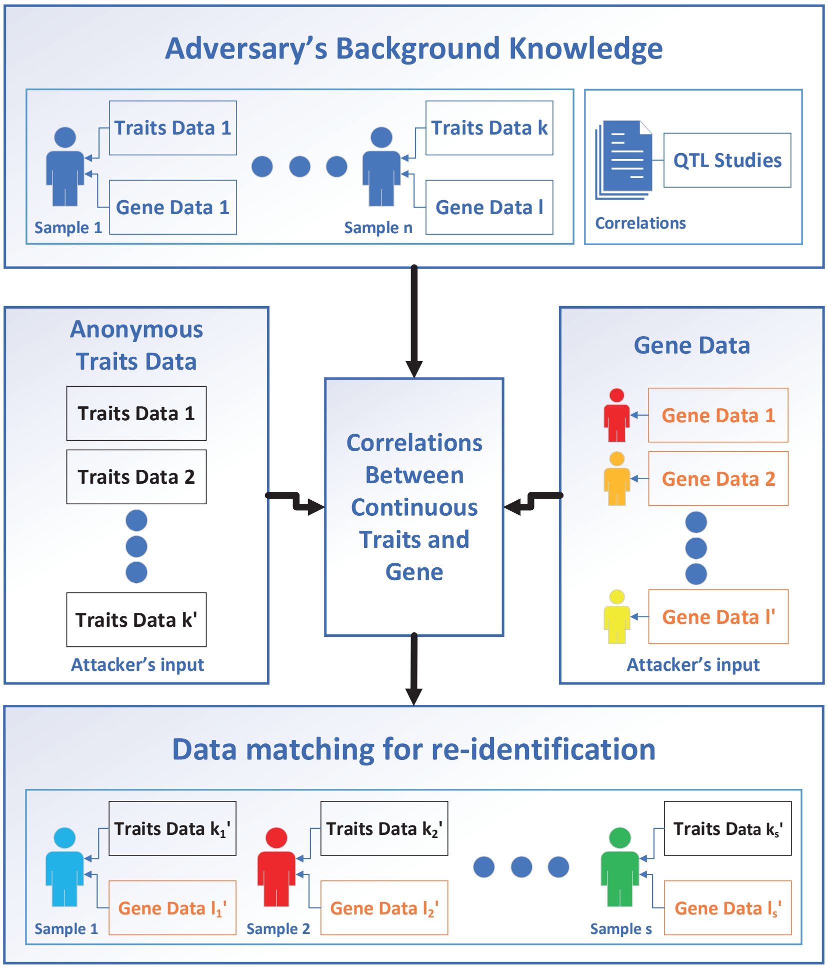

Figure 1. Privacy-breaching model for trait-gene profile reidentification. The adversary first infers the correlations between continuous trait data and gene data (central box) with training datasets (upper box left) or existing research results (upper box right) and then maps the anonymous continuous trait profile (coloured with black in the left box) to the genotype (coloured with orange in the right box) with correlation obtained for reidentification. Then, the adversary verifies whether an individual with the continuous trait data is the member of the genotype dataset. If the matching between the continuous trait profile and genotype is sufficiently significant, it is considered correct (lower box, reidentified individuals are indicated as human shapes with the same colour of that in the right box). Each human shape represent an individual; each trait data or gene data in a box represent a continuous trait profile or a genotype profile from an individual.

To make $\mathbb{S}(\Omega(i),\cdot)$ easier to handle, let $\mathbb{S}(\Omega(i),\cdot) \approx \mathbb{S}(i,\cdot)$, where the SNP represented by $\mathbb{S}(i,\cdot)$ is the SNP that most relevant to $\mathbb{T}(i,\cdot)$. Note that $i_1 \neq i_2 \Leftrightarrow \mathbb{T}(i_1,\cdot) \neq \mathbb{T}(i_2,\cdot), \mathbb{S}(i_1,\cdot) \neq \mathbb{S}(i_2,\cdot)$, then we have $m_s = m_t$ and $n_s = n_t$ for the training set. In Equation (1), $\Pr\left(S_{\Omega(i)} = \mathbb{S}(\Omega(i),k)\right)$ can be calculated using MAF, which is mentioned in Section 2.3, and may also be available from genetic database such as *dbSNP* [51]. $\Pr\left(T_i = \mathbb{T}(i,k) | S_{\Omega(i)} = \mathbb{S}(\Omega(i),k)\right)$ is characterized by a continuous conditional probability density $f_{T_i|S_{\Omega(i)}}$.

Both Michael Backes et al. [21] and Eric E Schadt et al. [20] verified that most of the continuous traits related to SNPs satisfied the normal distribution. However, unlike their solutions that used the normal distribution directly, since most continuous traits have non-negative values, the distribution with range $(0, +\infty)$ is more appropriate to model the continuous distribution functions. Specifically, let the mean and variance parameters of this truncated normal distribution be μ_i and σ_i, then its density is

$$f_{T_i|\mathbb{S}_{\Omega(i)}} = \frac{1}{\sigma_i}\frac{\phi\left(\frac{T_i-\mu_i}{\sigma_i}\right)}{1-\Phi\left(\frac{-\mu_i}{\sigma_i}\right)} = \frac{\phi\left(\frac{T_i-\mu_i}{\sigma_i}\right)}{\sigma_i\Phi\left(\frac{\mu_i}{\sigma_i}\right)}$$

where $\phi(\cdot)$ and $\Phi(\cdot)$ are the probability density function (p.d.f.) and cumulative distribution function (c.d.f.) respectively.

4.3. Matching Attack

After acquiring correlations $\Pr\left(T_i|S_{\Omega(i)}\right)$ for all pairs $\mathbb{T}(i,\cdot)$ and $\mathbb{S}(i,\cdot)$, we need to infer the individual links of the testing set between $m'_t \times n'_t$ continuous trait array $\mathbb{T}'$ containing $n'_t \geqslant 1$ members and $m'_s \times n'_s$ SNP array $\mathbb{S}'$ containing $n'_s \geqslant 1$ members. The members of $\mathbb{Q}'$ and $\mathbb{S}'$ may be different, where n'_t and n'_s are not necessarily equal; similarly with the training set, $\mathbb{T}(i,\cdot)$ and $\mathbb{T}'(i,\cdot)$ are corresponding to the same continuous trait, and $\mathbb{S}(i,\cdot)$ and $\mathbb{S}'(i,\cdot)$ are corresponding to the same SNP, then we have $m_s = m_t = m'_s = m'_t = m$.

The adversary needs to traverse the n'_t continuous trait samples and n'_s SNP samples to get the best match pairs $\{\mathbb{S}'(\cdot,l^*), \mathbb{T}'(\cdot,k^*)\}$. For any pair of $\{\mathbb{S}'(\cdot,l'), \mathbb{T}'(\cdot,k')\}$, The adversary first calculates the *trait propensity score* $e(l',k')_i$ for each pair of $\{\mathbb{S}'(i,l'), \mathbb{T}'(i,k')\}$ through correlations $\Pr\left(T_i|S_{\Omega(i)}\right)$, where $e(l',k')_i$ is defined as

$$e(l',k')_i = \Pr\left(S_{\Omega(i)} = \mathbb{S}'(i,l')|T_i = \mathbb{T}'(i,k')\right) \tag{2}$$

Next, the adversary calculates the *individual propensity score* $e(l',k')$ as

$$e(l',k') = \frac{1}{m}\sum_{i=1}^{m} e(l',k')_i \tag{3}$$

Finally, after traversing all the scores of SNP samples l' and continuous trait samples k^* paired, the adversary can know that the sample l^* that best matches sample k^* is

$$l^* = \arg\max_{l'} e(l',k^*) \tag{4}$$

4.4. Best Matching Validation

To evaluate the significance of the *individual propensity score*, we define *F Score* $F_{k'}$ for evaluation as

$$F_{k'} = \frac{e(l',k') - E[e(\cdot,k')]}{\mathrm{SD}[e(\cdot,k')]} \tag{5}$$

where $e(\cdot,k')$ is the set of traversed *individual propensity scores* between $\mathbb{T}'(\cdot,k')$ and $\mathbb{S}'$; $E[e(\cdot,k')]$ is the expectation of $e(\cdot,k')$, and $\mathrm{SD}[e(\cdot,k')]$ is the standard deviation of the set. In fact, the *F score* $F_{k'}$ is a standardized measurement for $e(l',k')$, which allows us to determine whether a continuous trait profile and its best-matched genotype are both from the same individual. Specifically, if $\mathbb{T}' \cap \mathbb{S}' = \varnothing$, the best matching score between the continuous trait profile and the SNP profile does not mean that these two profiles correspond to the same individual; in this case, we can detect these false positive matches with the *F score*. Moreover, even if n'_t-by-n'_s matching becomes computationally infeasible, it is possible to remove false positive matches with *F score*.

5. Synthetic Data Generation

There are few real-world datasets we can use to test the feasibility of the attack systematically because of two reasons. The first one is parameter control. The prior probabilities of the genes, the expectation and standard deviation of the continuous traits corresponding to the genes, etc., are uncontrollable in a real QTL dataset, which are not conducive to quantitative analysis of privacy risks. The second one is access control. Due to the current strict access control restrictions, it is difficult to obtain real QTL data for non-biological or non-medical research [52]. Therefore, synthetic data generation is necessary to quantify the privacy risks of continuous traits. The next two subsections will describe the design and implementation of the synthetic data generator respectively.

5.1. Design of the Synthetic Data Generator

We formulate the following rules for our synthetic data generators:

(a) Both continuous trait data and SNP data are sampled from the same population.
(b) Each trait in continuous trait data has one and only one corresponding SNP in SNP data, and different traits do not correspond to the same SNP, and vice versa.
(c) The continuous traits are related to SNP-based genes in three forms AA, AB, and BB, and the values of continuous traits corresponding to these three genotypes are all truncated normal distributions.

With these regulations, we will mention the implementation of our synthetic data generator in the next subsection.

5.2. Implementation of the Synthetic Data Generator

What our synthetic data generator needs to generate is the QTL dataset, which needs to generate the continuous trait data $\mathbb{T}^*$ and its corresponding SNP data $\mathbb{S}^*$. As described in our previous work [53], there are four steps for data generation:

First, we need to determine the structure of the dataset. Let $m_t^* = m_s^* = m, n_t^* = n_s^* = n$, and for $0 < i \leqslant m, 0 < j \leqslant n$, let $\mathbb{T}^*(\cdot, j)$ and $\mathbb{S}^*(\cdot, j)$ be the same individual and let $\Omega(i) = \mathbb{S}^*(i, \cdot)$, which means that the most correlated SNP of $\mathbb{T}^*(i, \cdot)$ is $\mathbb{S}^*(i, \cdot)$. Then we pre-set the parameters m, n for the synthetic data generator.

Next, we need to formalize the distributions of $\mathbb{T}^*(i, \cdot)$ corresponding with $\mathbb{S}^*(i, \cdot)$. We define $s_1, s_2, s_3 \in \{AA, AB, BB\} \wedge s_1 \neq s_2 \neq s_3$. For each pair of $\mathbb{T}^*(i, \cdot)$ and $\mathbb{S}^*(i, \cdot)$, there are three distributions $f_{T_i^*|s_1}, f_{T_i^*|s_2}, f_{T_i^*|s_3}$. The expectations of three distributions are randomly generated as $\mu_{T_i^*|s_1}, \mu_{T_i^*|s_2}, \mu_{T_i^*|s_3}$, such that $\mu_{T_i^*|s_1} < \mu_{T_i^*|s_2} < \mu_{T_i^*|s_3}$.

We thirdly define the distance between two distributions. The distance between the two expectations μ_1 and μ_2 does not reflect the distance between distributions f_1 and f_2; even if the absolute value $|\mu_2 - \mu_1|$ is very large, the larger standard deviations σ_1 and σ_2 will also make f_1 not far away from f_2. To accurately describe the distance between two distributions, we define the *z-score* z as the ratio between the difference of expectations $\mu_2 - \mu_1$ and the sum of standard deviations $\sigma_1 + \sigma_2$:

$$z = \frac{\mu_2 - \mu_1}{\sigma_1 + \sigma_2} \tag{6}$$

We also define z_α as the *z-score* of $f_{T_i^*|s_1}$ and $f_{T_i^*|s_2}$, z_β as the *z score* of $f_{T_i^*|s_2}$ and $f_{T_i^*|s_3}$. For each synthetic QTL dataset, all pairs of $\mathbb{T}^*(i, \cdot)$ and $\mathbb{S}^*(i, \cdot)$ in one QTL dataset use the same setting of z_α, z_β. Then we pre-set the parameters z_α, z_β for the synthetic data generator.

The final step is the generation of $\mathbb{T}^*(i, j)$ and $\mathbb{S}^*(i, j)$. Similarly with step 3, for each synthetic QTL dataset, all the $S(i, \cdot)$ use the same setting of MAF value p_{m} to obtain the prior probability. The synthetic data generator first randomly generates the value of $\mathbb{S}^*(i, j)$ as s_1, s_2, s_3 based on the prior probability $p_{s_1}, p_{s_2}, p_{s_3}$, and then generates $\mathbb{T}^*(i, j)$ through the corresponding probability distribution $f_{T_i^*|\mathbb{S}^*(i,j)}$. At last, we need to pre-set the parameters p_{m} for the synthetic data generator.

As can be seen from the steps above, we need five parameters $m, n, z_\alpha, z_\beta, p_\mathrm{m}$ as the input for the synthetic data generation in order to generate a synthetic QTL dataset. Referring to the findings from previous studies [21,34,35,54], we choose four values for m as 50, 100, 200, and 300, respectively, and four values for n as 50, 100, 200, and 500, respectively. Similarly, referring to the relationship between standard deviation and cumulative probability in the standard normal distribution, we choose six values for both z_α and z_β as 0.13, 0.68, 1.29, 1.65, 2.33, and 2.58, respectively, which are corresponding to cumulative probabilities as 55%, 75%, 90%, 95%, 99%, and 99.5%, respectively. For MAF values p_m, we choose 0.05, 0.15, 0.30, and 0.45, to roughly cover the value range of MAF ($0 < p_\mathrm{m} \leqslant 0.5$). After executing data generation, we obtain a 2304-item continuous trait dataset $\mathbb{T}^*$ and its corresponding SNP dataset $\mathbb{S}^*$ with the same item count. We repeat the data generation process 10 times, obtaining 10 $\mathbb{T}^*$ continuous trait datasets and 10 correlated $\mathbb{S}^*$ SNP datasets.

6. Attack Validation

We present our detailed experimental steps and main results here using the dataset described in Section 5. In this section, we first describe and quantify the degree of influences from different parameters, then identify the most important factors for continuous trait data re-identification based on mathematical derivation analysis, and finally use a real QTL dataset to evaluate the feasibility of our estimation.

6.1. Training and Testing Sets

Consulting the limitations of real QTL studies that the sample sizes of QTL datasets are always small (around 100) [21,50,54], we design two training/testing experimental setups as follows: (a) select half of the QTL profiles randomly as the training set if the sample size $n \leqslant 100$, and (b) select 50 QTL profiles randomly as the training set if the sample size $n > 100$.

After random splitting and training, we estimate the posterior probability by mapping $n/2$ ($n \leqslant 100$) or $n - 50$ ($n > 100$) continuous trait profiles for matching at a time with the n genotypes to evaluate the effectiveness of the re-identification attack. We repeat this splitting-training-matching process 5 times for each simulated QTL dataset (10 in total, mentioned in Section 5.2), resulting in 50 training/testing experiments for each parameter setting.

6.2. Matching Results

Since there are a large number of parameter settings, only typical results will be shown as figures. The matching accuracy with $z = 2.33$ are shown in Figure 2, which demonstrates several tendencies:

First, for all the SNP size m, the matching accuracy decreases as the size of the testing set increasing. Second, the matching accuracy decreases as the MAF value p_m decreases. This tendency appears in each sub-figure from Figure 2. If $p_\mathrm{m} \geqslant 0.30$, this tendency also holds in most cases, but occasionally the matching accuracy for an MAF of 0.45 drops blow 0.30. Third, the larger the *SNP sample size m*, the higher the matching accuracy.

Figure 3 shows the impact of different *z scores z* on the matching accuracy. When $z \geqslant 1.29$, the relationships between matching accuracy and z are close to '$z = 1.29$'; when $z = 0.13$ or $z = 0.68$, the matching accuracy has a cliff-like drop compared to $z \geqslant 1.29$, and all the error bars are becoming much longer, which implies that the matching accuracy of testing sets with these *z score* settings have great fluctuations. Moreover, the expectation of matching accuracy and MAF values are no longer positively correlated: the matching accuracy corresponding to $p_\mathrm{m} = 0.05$ and $p_\mathrm{m} = 0.15$ is higher than that of $p_\mathrm{m} = 0.30$ and $p_\mathrm{m} = 0.45$.

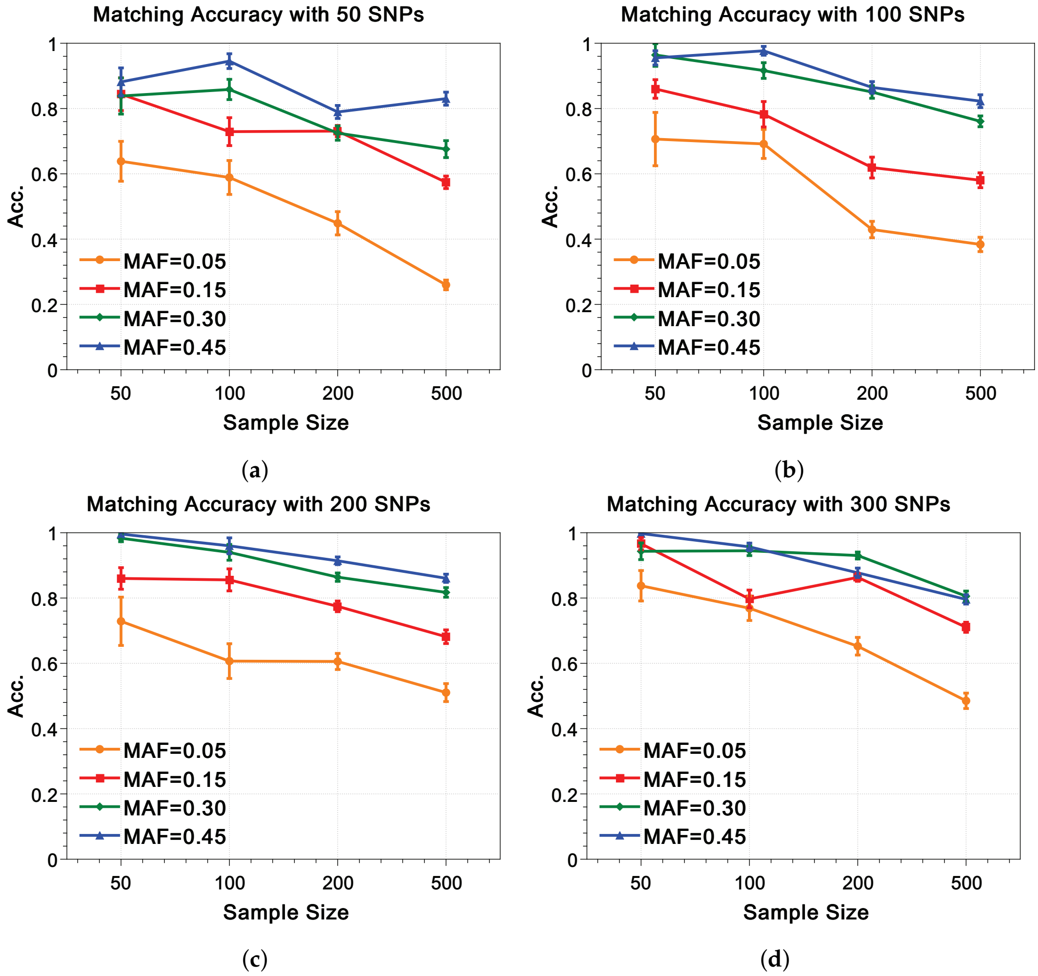

Figure 2. Matching accuracy with *z score* 2.33 **for both** z_α **and** z_β**.** The sample sizes n as 50, 100, 200, and 500 are expressed on the abscissa, respectively, while the matching accuracy is expressed on the ordinate. Matching accuracy with different MAFs and their standard deviations are expressed as different colored symbols with error bars, while the orange ellipse, red rectangle, olive diamond and blue triangle represent the MAF value of 0.05, 0.15, 0.30 and 0.45, respectively. The SNP sizes m of (**a**–**d**) are 50, 100, 200, and 300, respectively. (**a**) 50 SNP. (**b**) 100 SNP. (**c**) 200 SNP. (**d**) 300 SNP.

We also conduct the *F score* test, which is shown in Figure 4 as typical results. Figure 4a shows that it is impossible to reject most of the wrongly matched pairs while not rejecting a large proportion of correctly matched pairs when the MAF value $p_\mathrm{m} = 0.05$, regardless of the value of n. Figure 4c,d show that for $p_\mathrm{m} \geqslant 0.30$, there exists a value range of *F scores* that serves as a feasible threshold for distinguishing true positives (TPs) and false positives (FPs), where the lower bound of this threshold range is always 1.0. In addition, we tested the *F scores* with different values of m. Similarly to Figure 4, for an MAF value $p_\mathrm{m} = 0.30$ or $p_\mathrm{m} = 0.45$, a threshold of *F score* near 1.0 can distinguish TPs from FPs regardless of the values of m and n, which means that if the *F score* of the best matching is larger than threshold 1.0, then the trait profile and the SNP profile of this best matching can be considered as the same individual, and vice versa. Moreover, as m increases, the value range of the threshold becomes larger.

We know that m, n, z, p_m will affect the matching accuracy and the discrimination of true positive and false positive matching via the analysis above. The effect of m, n on the attack success rate is intuitive and easy to understand: the larger the m, the more accurate the correction of the overall prediction score; The larger the n, the more $\mathbb{S}^*(\cdot, j)$ needs to be matched, and then it is more likely to have matching errors. However, these conclusions are not sufficient to explain some of the phenomena presented in the figures above. One of the most important things is why MAF has such a significant impact on forecast matching accuracy. Another approach is that the prediction rate fluctuates greatly when the *z score* is not large (0.13 or 0.68). In the next subsections, unlike Lippert et al. [23] that only used experience-based statistical analysis, we will use the method of derivation to specifically analyze the reasons for these phenomena above.

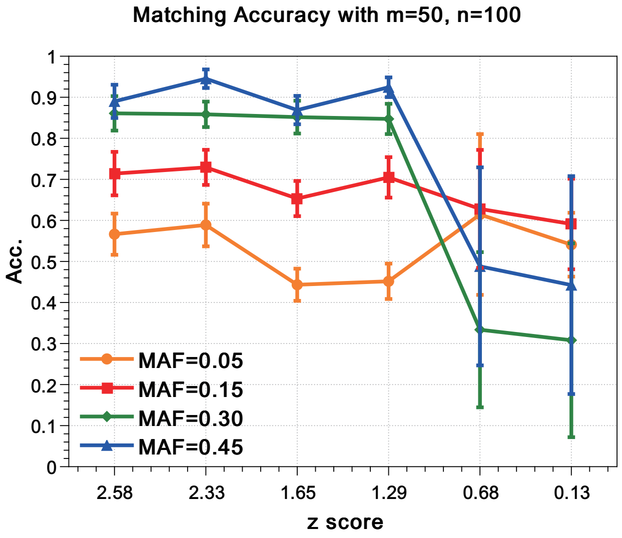

Figure 3. Matching Accuracy with $m = 50, n = 100$**.** The *z score* z as 0.13, 0.68, 1.29, 1.65, 2.33, and 2.58 are expressed on the abscissa, respectively, while the matching accuracy is expressed on the ordinate. Matching accuracy with different MAFs and their standard deviations are expressed as different colored symbols with error bars, while the orange ellipse, red rectangle, olive diamond and blue triangle represent the MAF values of 0.05, 0.15, 0.30 and 0.45, respectively.

6.3. Mathematical Analysis

The problem is that matching $\mathbb{T}^*(i,j')$ with $\mathbb{S}^*(i,j')$ is a single-feature ternary classification, which needs to be split into binary classification as pairwise combinations between $f_{T_i^*|s_1}, f_{T_i^*|s_2}, f_{T_i^*|s_3}$. In the following part of this subsection, we will analyze the single-feature binary classification, and then integrate the conclusions obtained into the single-feature ternary classification.

6.3.1. Binary Classification Analysis

We first approximate the truncated normal distribution to the normal distribution. Let the two probability density distribution functions $f_1(t)$ and $f_2(t)$ be normal distributions $\frac{1}{\sqrt{2\pi}\sigma_1}\exp(-\frac{(t-\mu_1)^2}{2\sigma_1^2})$ and $\frac{1}{\sqrt{2\pi}\sigma_2}\exp(-\frac{(t-\mu_2)^2}{2\sigma_2^2})$, then the joint probability density distributions with their prior probabilities p_1 and p_2 can be $p_1 f_1(t)$ and $p_2 f_2(t)$. When $p_1 f_1(t)$ and $p_2 f_2(t)$ are placed in the same coordinate system, there is a possibility that the two intersect, that is, $p_1 f_1(t) = p_2 f_2(t)$, which can be expanded as

$$\frac{p_1}{\sqrt{2\pi}\sigma_1}\exp(-\frac{(t-\mu_1)^2}{2\sigma_1^2}) = \frac{p_2}{\sqrt{2\pi}\sigma_2}\exp(-\frac{(t-\mu_2)^2}{2\sigma_2^2}) \tag{7}$$

where σ_1 and σ_2 are the standard deviations of $f_1(t)$ and $f_2(t)$, μ_1 and μ_2 are the expectations of $f_1(t)$ and $f_2(t)$, respectively.

To simplify Equation (7), we first define r as the ratio between σ_1 and σ_2 that $\sigma_2/\sigma_1 = r$, while p is the ratio between p_1 and p_2 that $p_2/p_1 = p$. Eliminate $1/\sqrt{2\pi\sigma}$ from both sides of the equation, then the Equation (7) can be changed as

$$\exp(-\frac{(t-\mu_1)^2}{2\sigma_1^2}) = \frac{p}{r}\exp(-\frac{(t-\mu_2)^2}{2r^2\sigma_1^2}) \tag{8}$$

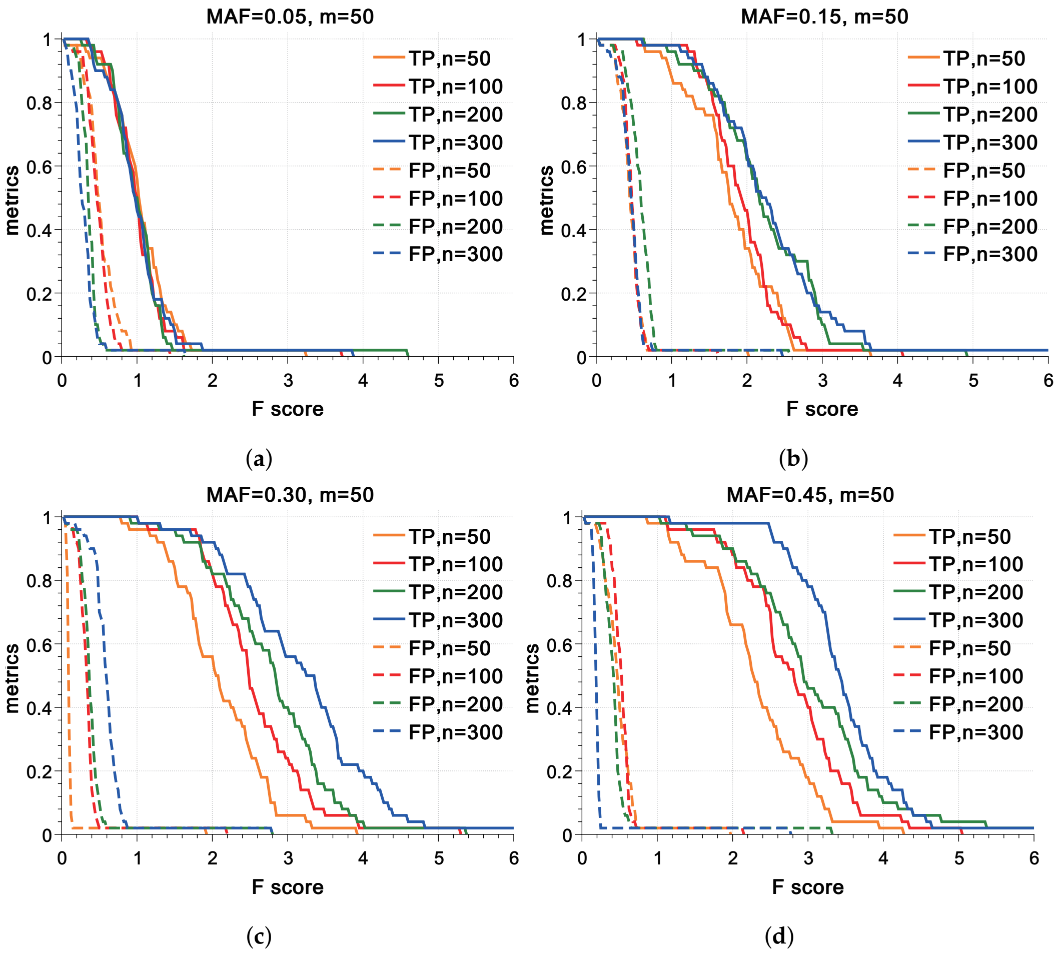

(**a**)

(**b**)

(**c**)

(**d**)

Figure 4. True-positive and false-positive for varying *F score* with SNP size 50 **and *z score*** 2.33**.** The abscissa values is *F score*, and the ordinate is metrics as percentage. Solid and dotted lines represent true-positive and false-positive, respectively. Different colours signify different sample sizes n, where orange represents $n = 50$, red represents $n = 100$, olive represents $n = 200$, and blue represents $n = 500$. Subfigures successively indicate MAF values p as 0.05, 0.15, 0.30, and 0.45. (**a**) 50SNP, 0.05 MAF. (**b**) 50SNP, 0.15 MAF. (**c**) 50SNP, 0.30 MAF. (**d**) 50SNP, 0.45 MAF.

Next, let $x = \frac{t-\mu_1}{\sigma_1}$, then we have

$$\exp(-\frac{x^2}{2}) = \frac{1}{r}\exp(-\frac{(x-\frac{\mu_2-\mu_1}{\sigma_1})^2}{2r^2}) \tag{9}$$

Finally, $\frac{t-\mu_2}{\sigma_2}$ can be transformed as $\frac{(x-(1+r)z)}{r}$ referring definition of *z score* as Equation (6) and r, with r, z, p we have

$$\exp(-\frac{x^2}{2}) = \frac{p}{r}\exp(-\frac{(x-(1+r)z)^2}{2r^2}) \tag{10}$$

Through the transformation above, we simplify six variables $\sigma_1, \sigma_2, \mu_1, \mu_2, p_1, p_2$ into three as r, z, p. Then finding the intersection between $p_1 f_1(t)$ and $p_2 f_2(t)$ is equivalent to finding the intersection between $p_1 f_1(x)$ and $p_2 f_2(x)$, or between $f_1(x)$ and $p f_2(x)$. Take the logarithm of both sides from Equation (10):

$$\frac{x^2}{2} - \frac{(x-(1+r)z)^2}{2r^2} = \ln\frac{r}{p} \tag{11}$$

Equation (11) is a quadratic equation for x, which can be converted to the form $ax^2 + bx + c = 0$:

$$(r^2-1)x^2+2(r+1)zx-[(1+r)^2z^2+2r^2\ln\frac{r}{p}]=0 \tag{12}$$

$b^2-4ac \geqslant 0$ is the condition under which Equation (12) has solutions, which can be represented as

$$b^2-4ac=4r^2(r+1)^2(z^2+2\times\frac{r-1}{r+1}\times\ln\frac{r}{p}) \tag{13}$$

Obviously $r>0$, so $r^2>0$, $(r+1)^2>0$, then the case where $p_1f_1(x)$ and $p_2f_2(x)$ have intersections can be expressed as

$$z^2+2\times\frac{r-1}{r+1}\times\ln\frac{r}{p}\geqslant 0 \tag{14}$$

It needs to be divided into two cases to discuss: $0<r<1$ and $r>1$. For $0<r<1$, we have $\frac{r-1}{r+1}<0$. If $p>r\times\exp(\frac{z^2(r+1)}{2(r-1)})$, then $\ln\frac{r}{p}<0$, $\frac{r-1}{r+1}\times\ln\frac{r}{p}>0$, $p_1f_1(x)$ and $p_2f_2(x)$ always have intersections; similarly, for $r>1$, we have $\frac{r-1}{r+1}>0$. If $p<r\times\exp(\frac{z^2(r+1)}{2(r-1)})$, then $\ln\frac{r}{p}>0$, $\frac{r-1}{r+1}\times\ln\frac{r}{p}>0$, we still have the conclusion that $p_1f_1(x)$ and $p_2f_2(x)$ always have intersections. Then we should have

$$p\begin{cases}\geqslant r\times\exp(\frac{z^2(r+1)}{2(r-1)}) & 0<r<1\\ \leqslant r\times\exp(\frac{z^2(r+1)}{2(r-1)}) & r>1\end{cases} \tag{15}$$

to make $b^2-4ac\geqslant 0$. Figure 5 is a typical example for $f_1(x)$, $f_2(x)$, $p_1f_1(x)$, and $p_2f_2(x)$ with given r,z,p. In this example the r,z,p fix Equation (15), so we have $p_2f_2(x)>p_1f_1(x)$ when $x_1<x<x_2$, where x_1,x_2 is the solution of Equation (12) and $x_1<x_2$. Let f_1,f_2 be $f_{T_i^*|s_1}, f_{T_i^*|s_2}$, respectively, the privacy breaching method will match $\mathbb{T}^*(i,j')$ to a $\mathbb{S}^*(i,l')$ with value s_2 when $\mathbb{T}^*(i,j')$ is in the interval (x_1,x_2). If r,z,p do not fix Equation (15), for example $p=0.1$, we have $p_2f_2(x)<p_1f_1(x)$ for any x, then the privacy breaching method will only match $\mathbb{T}^*(i,\cdot)$ to the same value s_1 in $\mathbb{S}^*(i,\cdot)$, which makes s_2 indistinguishable.

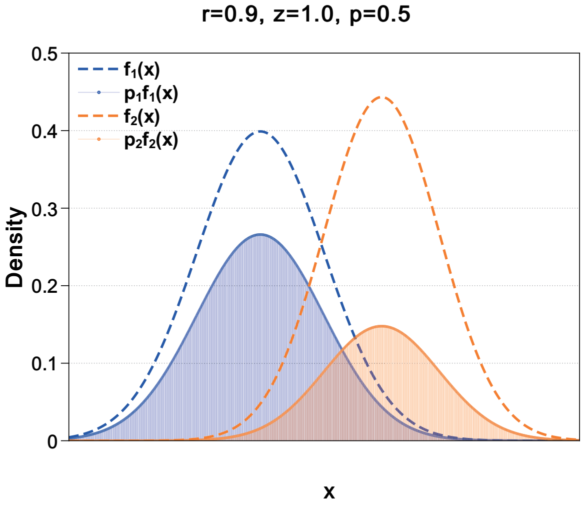

Figure 5. Schematic diagram of the probability density distribution of x when $r=0.9, z=1.0$, $p=0.5$. The horizontal coordinate axis is x, while the vertical coordinate axis is the probability density. Blue and orange dashed lines are curves of function $f_1(x)$ and $f_2(x)$, respectively, while the blue and orange solid lines are curves of function $p_1f_1(x)$ and $p_2f_2(x)$, respectively. The areas of the blue and orange regions are integrals of $f_1(x)$ and $f_2(x)$, respectively.

Next, we discuss how distinguishable s_1 and s_2 are. Let the area of the blue part be A_b, and the area of the orange part be A_o. It is obvious that $A_b=p_1$, $A_o=p_2$. The area where the blue part does not overlap with the orange part is A_{b-o}; similarly, the area where the orange part does not overlap with the blue part is A_{o-b}. As shown in Figure 5, the theoretical minimum error probability is given by the area under the minimum value of the two curves, which is the area of the overlapping area of blue and orange $A_{b\cap o}$.

For a given point x, the best theoretical error probability is given by the less likely one of the two classes:

$$\Pr(wrong|x) = \min(p_1 f_1(x), p_2 f_2(x))\mathrm{d}x \tag{16}$$

Then it can be integrated over the population to get the total error probability:

$$A_{b\cap o} = \int_{-\infty}^{+\infty} \min(p_1 f_1(x), p_2 f_2(x))\mathrm{d}x \tag{17}$$

According to Equation (17), we can obtain the area of A_{b-o} and A_{o-b} as

$$\begin{aligned} A_{b-o} &= A_b - A_{b\cap o} \\ A_{o-b} &= A_o - A_{b\cap o} \end{aligned} \tag{18}$$

A_{b-o}, A_{o-b} and $A_{b\cap o}$ are corresponding to important indicators in statistical analysis, where A_{o-b} is true positive (TP), A_{b-o} is true negative (TN), and $A_{b\cap o}$ is corresponding to both false positive (FP) and false negative (FN). Through these indicators we can use the relevant basic concepts of statistical analysis more directly, such as positive rate (TPR) or *sensitivity*, true negative rate (TNR) or *speciality*, and *accuracy*; the *accuracy* Acc* and *sensitivity* Sen* can be calculated as follows:

$$\begin{aligned} \mathrm{Acc}^* &= \frac{A_{b-o} + A_{o-b}}{A_{b-o} + A_{o-b} + 2A_{b\cap o}} \\ \mathrm{Sen}^* &= \frac{A_{o-b}}{A_o} \end{aligned} \tag{19}$$

Substituting different r, z, p combinations into Equation (19) shows that the *accuracy* and *sensitivity* are not positively correlated. Figure 6 is a typical example. Figure 6b shows that when $0 < r < 1, z = 0.5$, the *sensitivity* decreases monotonically with the decrease of p. However, Figure 6a shows that with the same conditions, the *accuracy* does not decrease monotonically with the decrease of p: there are inflection points for each curve. When p becomes small enough, the *accuracy* will be very close to 100%, while the truncated curve means that r, z, p do not fix Equation (15) if p is smaller than the breakpoint. In this situation, the *sensitivity* is 0.

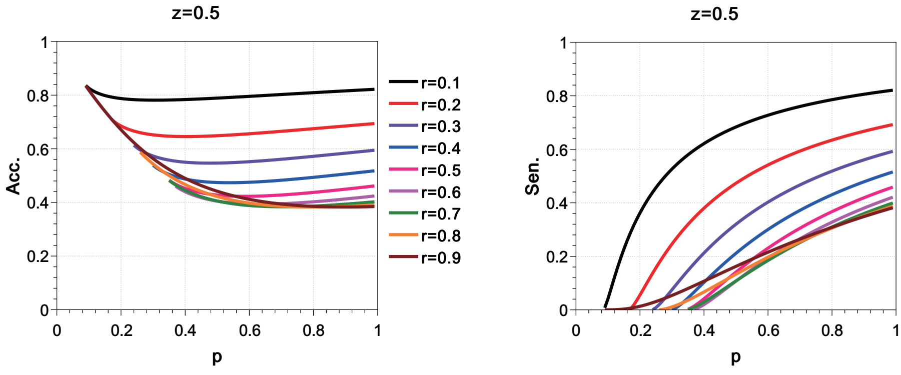

(**a**) (**b**)

Figure 6. ***Accuracy* and *sensitivity* of binary classification with $z = 0.5$.** The horizontal coordinate axis is p, while the vertical coordinate axis is the value of *accuracy* and *sensitivity*. The curves represented by different r values are distinguished by different colors. (**a**) Accuracy. (**b**) Sensitivity.

The principle of privacy breaching attack is matching $\mathbb{T}^*(\cdot, j')$ to $\mathbb{S}^*(\cdot, l')$ with the highest average *accuracy*. If the *sensitivity* is too small (nearly 0) for matching most of the $\mathbb{S}^*(i,\cdot)$ with $\mathbb{T}^*(i,\cdot)$, the privacy breaching attack will match $\mathbb{T}^*(\cdot,j')$ to the same SNP profile with possibly high *accuracy*, which results in matching the vast majority $\mathbb{T}^*(\cdot,j')$ to an error $\mathbb{S}^*(\cdot,l')$. For a privacy breaching attack, it is more important to be able to distinguish $\mathbb{S}^*(\cdot,l')$ by $\mathbb{T}^*(\cdot,j')$, therefore the matching accuracy should be mainly related to *sensitivity*.

We test different r, z, and p in Equation (19) and found interesting correlations between these three parameters and *sensitivity*. Figure 7 shows the changing trend of *sensitivity* with $0 < r < 1$, $0 < z < 1$, and $0 < p < 1$ very intuitively. Empty positions indicate that the *sensitivity* there is 0. The boundary with the *sensitivity* of 0 is a saddle-shaped cambered surface. The sensitivity of the side of the cambered surface face to $p = 0, z = 0$ is 0; on the other side of the cambered surface, the farther away from the surface, the higher the *sensitivity*.

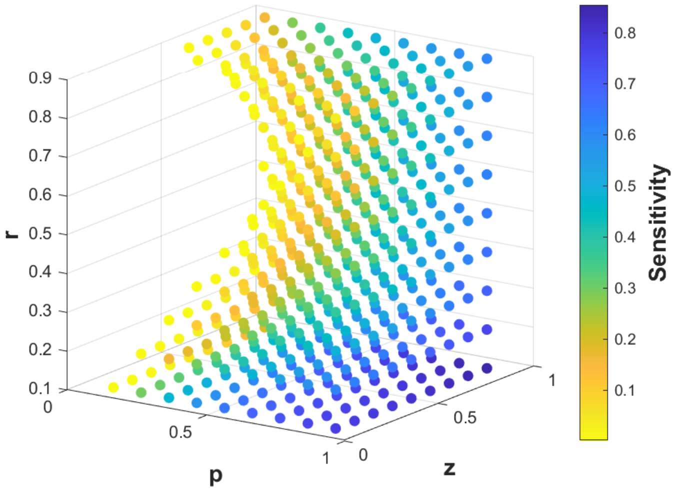

Figure 7. *Sensitivity* with different r, z, and p. The three coordinates represent r, z, and p, respectively. *Sensitivity* is represented by different colors. The deeper the color, the higher the *sensitivity*. The vacant parts indicate that the *sensitivity* is zero when r, z, p take the corresponding values.

6.3.2. Ternary SNP-Based Classification Analysis

Similarly with the derivation process for binary classification, let the prior probabilities of distributions $f_1(t)$, $f_2(t)$, and $f_3(t)$ be p_1, p_2, and p_3, respectively, then the intersection points t between joint distribution $p_1 f_1(t)$, $p_2 f_2(t)$ and $p_3 f_3(t)$ can be represented as

$$\begin{aligned}
\frac{p_1}{\sqrt{2\pi}\sigma_1}\exp(-\frac{(t-\mu_1)^2}{2\sigma_1^2}) &= \frac{p_2}{\sqrt{2\pi}\sigma_2}\exp(-\frac{(t-\mu_2)^2}{2\sigma_2^2}) \\
\frac{p_1}{\sqrt{2\pi}\sigma_1}\exp(-\frac{(t-\mu_1)^2}{2\sigma_1^2}) &= \frac{p_3}{\sqrt{2\pi}\sigma_3}\exp(-\frac{(t-\mu_3)^2}{2\sigma_3^2}) \\
\frac{p_2}{\sqrt{2\pi}\sigma_2}\exp(-\frac{(t-\mu_2)^2}{2\sigma_2^2}) &= \frac{p_3}{\sqrt{2\pi}\sigma_3}\exp(-\frac{(t-\mu_3)^2}{2\sigma_3^2})
\end{aligned} \tag{20}$$

Let $r_\alpha = \frac{\sigma_2}{\sigma_1}, r_\beta = \frac{\sigma_3}{\sigma_1}, r_\gamma = \frac{\sigma_3}{\sigma_2}$, then we have $r_\gamma = \frac{r_\beta}{r_\alpha}$. With MAF value p_m and the definition of MAF from Section 2.3, p_1, p_2, and p_3 can be represented as $p_1 = (1-p_\mathrm{m})^2$, $p_2 = 2p_\mathrm{m}(1-p_\mathrm{m})$, and $p_3 = p_\mathrm{m}^2$. Let $p_\alpha = \frac{p_2}{p_1}, p_\beta = \frac{p_3}{p_1}, p_\gamma = \frac{p_3}{p_2}$, then we have $p_\alpha = \frac{2p_\mathrm{m}}{1-p_\mathrm{m}}, p_\beta = (\frac{p_\mathrm{m}}{1-p_\mathrm{m}})^2, p_\gamma = \frac{p_\mathrm{m}}{2(1-p_\mathrm{m})}$. To simplify $p_\alpha, p_\beta, p_\gamma$, let $\frac{p_\mathrm{m}}{1-p_\mathrm{m}} = p_\mathrm{st}$, then we have $p_\alpha = 2p_\mathrm{st}, p_\beta = p_\mathrm{st}^2, p_\gamma = \frac{p_\mathrm{st}}{2}$. For the values of z, Let $z_\alpha = \frac{\mu_2-\mu_1}{\sigma_1+\sigma_2}, z_\beta = \frac{\mu_3-\mu_1}{\sigma_1+\sigma_3}$, $z_\gamma = \frac{\mu_3-\mu_2}{\sigma_2+\sigma_3}$, then z_γ can be represented as $z_\gamma = [(1+r_\beta)z_\beta - (1+r_\alpha)z_\alpha]/(1+r_\beta/r_\alpha)$. Finally let $x = \frac{t-\mu_1}{\sigma_1}$, and substitute $r_\alpha, r_\beta, p_\mathrm{st}, z_\alpha, z_\beta$ into Equation (20), then we have three quadratic equations:

$$
\begin{aligned}
(r_\alpha^2-1)x^2+2(r_\alpha+1)z_\alpha x-[(1+r_\alpha)^2z_\alpha^2+2r_\alpha^2\ln\frac{r_\alpha}{2p_{\rm st}}]=0\\
(r_\beta^2-1)x^2+2(r_\beta+1)z_\beta x-[(1+r_\beta)^2z_\beta^2+2r_\beta^2\ln\frac{r_\beta}{p_{\rm st}^2}]=0\\
(\frac{r_\beta^2}{r_\alpha^2}-1)x^2+2[(1+r_\beta)z_\beta-(1+r_\alpha)z_\alpha]x\\
-\{[(1+r_\beta)z_\beta-(1+r_\alpha)z_\alpha]^2+2\frac{r_\beta^2}{r_\alpha^2}\ln\frac{2r_\beta}{p_{\rm st}r_\alpha}\}=0
\end{aligned}
\tag{21}
$$

Equation (21) shows that for each pair $\{\mathbb{T}^*(i,\cdot),\mathbb{S}^*(i,\cdot)\}$, there are three *sensitivity* values, which are determined by five parameters $z_\alpha, z_\beta, r_\alpha, r_\beta, p_{\rm m}$. Our synthetic data was generated without considering the factor r, hence $z_\alpha, z_\beta, p_{\rm m}$ of the synthetic data are pre-set while r_α, r_β are random, which can explain the fluctuation of the matching accuracy in Figure 3. Figure 7 shows that a change in r will have a significant impact on *sensitivity* when the value of z is not high, while it has less effect on *sensitivity* if the value of z is high enough, which fix our matching accuracy results appropriately. Similarly, if $p_{\rm m}$ is low, $p_\alpha, p_\beta, p_\gamma$ will all be small values, resulting in a low *sensitivity* in most cases even r_α, r_β are floating.

6.3.3. Sensitivity Score of Synthetic Data

We combine the results of binary classification to the case of ternary SNP-based classification. For i-th continuous trait with its most correlative SNP, we define its *sensitivity score* Sen_i as

$$\mathrm{Sen}(i)=\min(\mathrm{Sen}(i,\cdot)) \tag{22}$$

where $\mathrm{Sen}(i,\cdot)$ is the sensitivity calculated by Equation (21) with pairwise combinations between $f_{Q_i|s_1}, f_{Q_i|s_2}, f_{Q_i|s_3}$ as $\{f_{Q_i|s_1}, f_{Q_i|s_2}\}$, $\{f_{Q_i|s_1}, f_{Q_i|s_3}\}$ and $\{f_{Q_i|s_2}, f_{Q_i|s_3}\}$ from i-th continuous trait. Then the *data sensitivity score* Sen can be calculated as

$$\mathrm{Sen}=\frac{1}{m}\sum_{i=1}^{m}\min(\mathrm{Sen}(i,\cdot)) \tag{23}$$

We calculate the Sen of all our synthetic data. Typical results are shown in Figure 8. Similar to the conclusion that can be drawn from Figure 7, the larger the z, the higher the Sen; the smaller the $p_{\rm m}$, the lower the Sen. However, the sample size n can also influence Sen. *Data sensitivity score* decreases as n increases when $p_{\rm m}$ is small ($p_{\rm m}=0.05, p_{\rm m}=0.15$); if $p_{\rm m}$ is large, the *data sensitivity score* is basically not affected by the change of n. The most likely reason is undersampling. If the sample size of synthetic data is small, undersampling is prone to occur for small $p_{\rm m}$, resulting in a falsely high *data sensitivity score*; as n increases, the probability of undersampling becomes lower, and the *data sensitivity score* is no longer artificially high. In contrast, datasets with $p_{\rm m}\leqslant 0.30$ are not prone to undersampling when n is small, therefore the *data sensitivity score* is relatively stable. In addition, for our privacy breaching method, when the MAF value $p_{\rm m}$ is small, the increase of n mainly leads to a significant difference between the *sensitivity* of the matching set and the training set, which is also the main reason that the smaller the MAF, the more obvious the matching accuracy declines with the increase of n.

Figure 8 also demonstrates the phenomenon that the ability to distinguish TP and FP matching by *F score* does not only correlate significantly with the *data sensitivity score*. Even though the value of the *sensitivity score* is up to 0.9 as shown in Figure 8b with MAF value $p_{\rm m}=0.05$, it is still hard to find an effective threshold for distinguishing. It is speculated that the discrimination rate of TP and FP matching by *F score* is most positively correlated with the absolute value of A_{0-b}, or more precisely $E[\mathrm{Sen}(i,\cdot)\times p_{\rm m}^2]$. Since the main factor affecting the value of A_{0-b} is $p_{\rm m}^2$, the discrimination rate of TP and FP matching by *F score* is mainly related to $p_{\rm m}$.

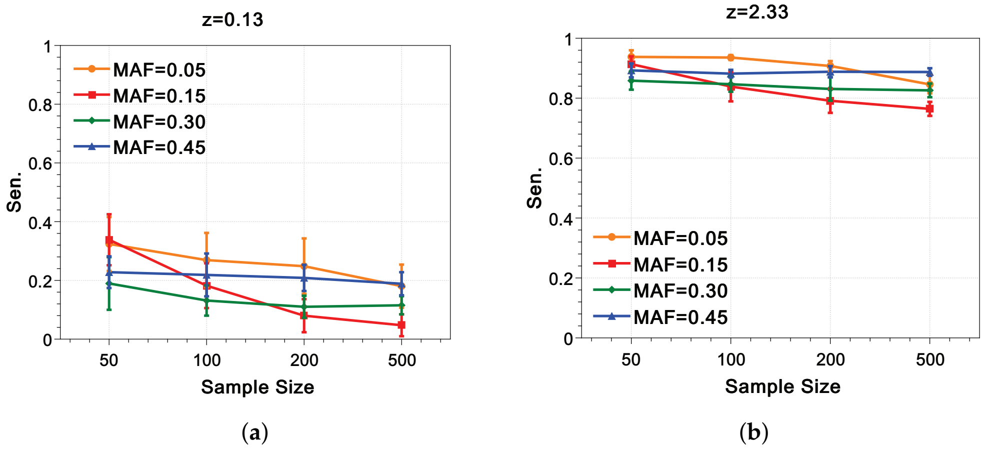

Figure 8. ***Sensitivity score*** **Sen with SNP size** $m = 50$**.** The sample sizes n as 50, 100, 200, and 500 are expressed on the abscissa, respectively, while the matching accuracy is expressed on the ordinate. Matching accuracy with different MAFs and their standard deviations are expressed as different colored symbols with error bars, while the orange ellipse, red rectangle, olive diamond and blue triangle represent the MAF value of 0.05, 0.15, 0.30 and 0.45, respectively. (**a**,**b**) indicate z of 0.13 and 2.33, respectively. (**a**) $z = 0.13$. (**b**) $z = 2.33$.

6.3.4. Overall Analysis

From the experimental results and mathematical analysis above, to judge whether $\mathbb{T}'(\cdot, k')$ in a continuous trait dataset $\mathbb{T}'$ can effectively match a SNP sample $\mathbb{S}'(\cdot, l')$, there are three major aspects as follows:

(a) Both the SNP size m and the *data sensitivity score* of the QTL dataset $\mathbb{T}'$ are most positively correlated with matching accuracy. The larger the m and *data sensitivity score* Sen related to the r, z, p of each $\mathbb{T}'(i, \cdot)$, the higher the matching accuracy.

(b) The discrimination rate of TP and FP matching between $\mathbb{T}'$ and $\mathbb{S}'$ by *F score* is most positively correlated with the MAF value $p_{\rm m}$ and will be affected by m to some extent. The larger the MAF, the easier to distinguish between TP and FP matching.

(c) The sample size n significantly affects matching accuracy, especially when the MAF value is small. The larger n, the lower the matching accuracy.

The sample size n, the SNP size m, and the *data sensitivity score* Sen can be used to predict the approximate range of matching accuracy; m and MAF value $p_{\rm m}$ can be used to estimate the discrimination rate of TP and FP matching by *F score*. In the next subsection, we will verify the effectiveness of these three major aspects in predicting the privacy risk of a real QTL dataset.

6.4. Real Data

We use a real QTL dataset to verify the validity of major factors summarized in the previous Section 6.3.4. The real dataset *CSF pQTL study in the Japanese population* used in this study consists of proteomics and SNPs publicly available in the gene expression omnibus (GEO) database under references GSE83708, GSE83709 and GSE83710. GSE83708 represents the SNPs of 89 samples with genotyping Q17, GSE83709 represents the SNPs of 44 samples with genotyping Q35, and GSE83710 is the proteomic data of all 133 samples, which were collected between May 2010 and February 2014 at the National Center Hospital, National Center of Neurology and Psychiatry, Kodaira, Tokyo, Japan [48]. The entire dataset contains the relative fluorescence units (RFU) of the cerebrospinal fluid (CSF) levels of 1126 proteins in 133 subjects and 954,703 SNPs.

Analysis by previous researchers [48] revealed that a total of 421 cis and 25 trans SNP-protein pairs were significantly correlated at a false discovery rate (FDR) of less than 0.01 ($P_{nominal} < 7.66 \times 10^{-9}$); cis-only analysis revealed an additional 580 significant cis SNP-protein pairs with an FDR < 0.01 ($P_{nominal} < 2.13 \times 10^{-5}$). All the data can be downloaded from the National Center for Biotechnology Information (NCBI) database.

6.5. Privacy Risk Estimation

We keep only the most correlated SNP for each protomic trait, resulting in 62 pairs of continuous trait and SNP based on previous work [48]. The matching accuracy and standard deviation for these 62 pairs are shown in Table 1:

Table 1. Matching Accuracy (MA) and *F score* for Real Data Matching

MA	MA Std	*F score*	*F score* Std
0.2255	0.0385	1.8747	0.7421

Even though there are strong correlations between traits and genotypes as $P_{nominal}$ measured, the matching accuracy is still very low, which shows that the matching accuracy is not necessarily positively correlated with the correlations between traits and SNPs measured by $P_{nominal}$.

As Section 6.3.4 mentioned, there are three major aspects that affect matching accuracy and the discrimination rate of TP and FP matching. For the first major aspect, we calculate the *data sensitivity score* Sen of this real data and found it to be 0.2074, which is close to the Sen of $z = 0.13$ in Figure 8. The lower value of Sen is also consistent with condition that most of the *z score* (more than 70%) is low (less than 1.29) as Figure 9b shows. The m of the real data is 62, which is close to the lowest m of our synthetic data. From the inference *a* in Section 6.3.4, low values of m and Sen will lead to low matching accuracy, and the actual matching accuracy from Table 1 shows that our inference is in line with the actual situation. For the second major aspect, it can be seen from Figure 9a that the MAF value $p_{\mathrm{m}} \geqslant 0.30$ of nearly 70% of the SNPs, so the discrimination rate between TP and FP matching should be high, which is also consistent with the results of *F score* in Table 1 (mostly upper than 1.0). For the last major aspect, the n of the real data is 133, which is close to $n = 100$ and means that the reliability needs to be improved. Combine these three aspects and match m, n, z to where $m = 50, n = 100, z = 0.13$ as shown in Figure 3, results show that there is a corresponding relationship between the matching accuracy of real data and synthetic data. Analysis of real data indicates that the three major aspects are effective in predicting privacy risk.

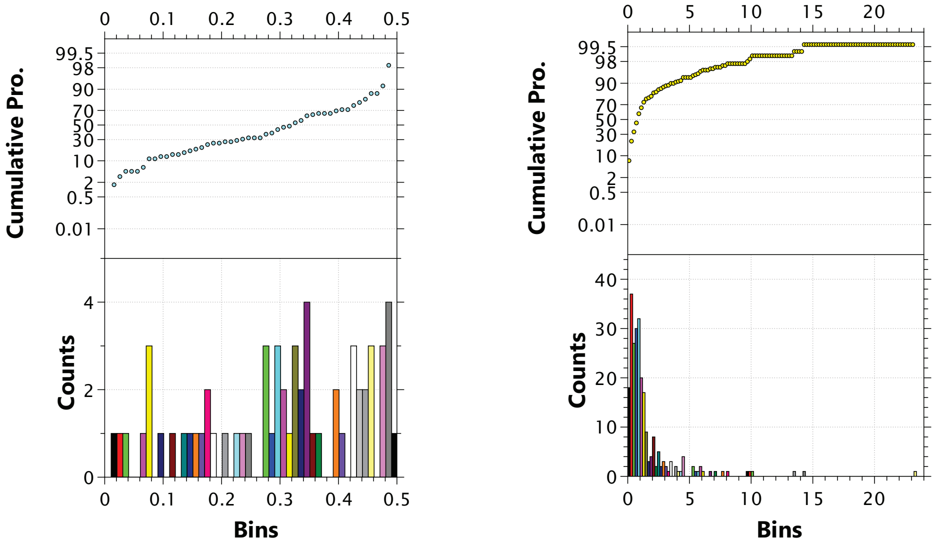

(**a**) (**b**)

Figure 9. Counts and cumulative probability of the MAF values (a) and *z scores* (b) of the real data. The abscissa is the MAF values and *z scores*, the lower half of the ordinate is the number of MAFs/*z scores* in each interval of the histogram, and the upper half of the ordinate is the cumulative probability of each interval in the histogram. (**a**) MAF analysis. (**b**) z_{α} and z_{β} analysis.

7. Discussion

The quantitative analysis we have proposed is not only for the possibility of privacy threats, but more importantly, for the probability of privacy risks for continuous trait data. Based on our findings from Section 6, we can classify the privacy risk by predicting the matching accuracy of the continuous trait data, so as to maximize the benefits of data sharing under the premise of ensuring data privacy. For example, we can divide the privacy risks of the continuous trait dataset into low, medium and high levels through the *sensitivity score* ($\text{Sen} \leqslant 0.25, 0.25 < \text{Sen} \leqslant 0.50, \text{Sen} > 0.50$). For the low-level data, we can adopt the form of resource disclosure that continuous trait data resources can be used and shared at any time with just anonymized. For the medium-level data, we need to adopt the form of platform collaborative data sharing, which should be based entirely on the sharing platform for cooperation; data should only be circulated and shared through the platform, while the shared data should not flow out of the collaborative data platform. For the high-level data, we must adopt the method of peer-to-peer data cooperation and adopt the cooperation principle of one discussion for one case. The cooperation application should include the description of both parties, the basis of cooperation, the purpose of cooperation, the mode of cooperation, the results of cooperation and the purpose of use, etc. In addition, the data provider also needs to add as much noise as possible to the trait data under the premise of ensuring availability according to the purpose of the cooperation.

Considering the influence of other factors, m, p_m and n are required to make corrections to the privacy risks. If $m \leqslant 200$, the privacy risks will be increased by one level base on Sen; similarly, if the proportion of SNPs with MAF value $p_\text{m} < 0.25$ in QTLs is greater than 50%, the privacy risks will be lowered by one level. Furthermore, if the QTL sample size is lower than 100, the privacy risks of the dataset should be preset to only medium and high levels.

8. Conclusions

We have presented a re-identification attack via simulated genotype data and showed that the matching SNP size is one of the major factors that can be used to quantify both genomic privacy breaching accuracy and the discrimination rate of TP and FP matching.

Then, by implementing a mathematical analysis of the distribution characteristics of our synthetic data, we demonstrated that the *sensitivity*, which is the main factor affecting the matching accuracy, is dependent on the ratio of standard deviation, the relative distance of expectation, and the ratio of prior probability, between different distributions with the same trait. Different from *sensitivity*, the MAF value is the main factor affecting the discrimination rate. Additionally, the size of the matching set will significantly affect the evaluation accuracy of privacy concerns in practical situations.

Finally, a matching test with real data led to the conclusion that our evaluation criteria are effective in predicting the privacy risks of gene-related continuous trait data.

Although our approach to assessing the privacy implications of continuous trait datasets has been shown to be effective, the present study has the following limitations, which need to be addressed in future studies.

First, the parameter setting of the simulated data needs to be more refined. Ratios between standard deviation r_α and r_β should be more specific. Furthermore, since the distributions of r_α and r_β were not specified when the data had been generated, the matching accuracy in Figures 2 and 3 did not decrease monotonically with the increase of n and z but fluctuates, which was more likely to be related to the random distribution of r_α and r_β. For the further studies, we will focus on analyzing how different r will affect the *sensitivity score* and the effectiveness of the privacy breaching.

Second, sampling method for synthetic data generation needs to be improved. 50 times for sampling and training is inability to show hidden dangers accurately when faced with smaller MAFs. In the following studies we will increase the number of samples and increase the sample size of the training set. Furthermore, we will expand the value range of parameters to know under what conditions the privacy breaching attack can achieve the effect of the real data used in the prevous work [20,21].

Finally, the method of calculating the *sensitivity score* $\mathrm{Sen}(i)$ that for the ternary classification needs to be improved. The existing solution only considers the impact of the lowest Sen on the matching accuracy, but in actual cases, the impact of the second lowest Sen needs to be validated. In future studies we will estimate the impact of the second lowest Sen with more refined parameter settings.

Author Contributions: Conceptualization, M.H.; Data curation, M.H.; Formal analysis, M.H. and W.W.; Investigation, M.H.; Methodology, S.X.; Project administration, W.Q. and H.J.; Resources, D.Z., W.Q. and H.J.; Supervision, D.Z.; Visualization, S.X.; Writing—original draft, M.H.; Writing—review & editing, S.X. and W.W. All authors have read and agreed to the published version of the manuscript.

Funding: This research received no external funding.

Institutional Review Board Statement: Not applicable.

Informed Consent Statement: Not applicable.

Data Availability Statement: Not applicable.

Conflicts of Interest: The authors declare no conflict of interest. The funders had no role in the design of the study; in the collection, analyses, or interpretation of data; in the writing of the manuscript; or in the decision to publish the results.

References

1. The International HapMap Consortium. The international HapMap project. *Nature* **2003**, *426*, 789. [CrossRef]
2. Todorovic, V. Publisher Correction: Amplification-free single-cell whole-genome sequencing gets a makeover. *Nat. Methods* **2020**, *17*, 242. [CrossRef] [PubMed]
3. Lappalainen, T.; Scott, A.J.; Brandt, M.; Hall, I.M. Genomic analysis in the age of human genome sequencing. *Cell* **2019**, *177*, 70–84. [CrossRef] [PubMed]
4. Gawad, C.; Koh, W.; Quake, S.R. Single-cell genome sequencing: Current state of the science. *Nat. Rev. Genet.* **2016**, *17*, 175. [CrossRef] [PubMed]
5. Bush, W.S.; Moore, J.H. Genome-wide association studies. *PLoS Comput. Biol.* **2012**, *8*, e1002822. [CrossRef] [PubMed]
6. Chen, G.; Wang, C.; Shi, T. Overview of available methods for diverse RNA-Seq data analyses. *Sci. China Life Sci.* **2011**, *54*, 8. [CrossRef] [PubMed]
7. Genome-Wide Association Studies. Available online: https://www.mgi-tech.com/applications/info/8/ (accessed on 1 January 2020).
8. 23 and Me Research Innovation Collaborations Program. Available online: https://research.23andme.com/research-innovation-collaborations/ (accessed on 1 January 2020).
9. Kraft, P.; Haiman, C.A. GWAS identifies a common breast cancer risk allele among BRCA1 carriers. *Nat. Genet.* **2010**, *42*, 819–820. [CrossRef]
10. Fachal, L.; Dunning, A.M. From candidate gene studies to GWAS and post-GWAS analyses in breast cancer. *Curr. Opin. Genet. Dev.* **2015**, *30*, 32–41. [CrossRef]
11. Wang, X.F.; Zhou, X.; Rao, J.H.; Zhang, Z.J.; Yang, Y.D. Imputing DNA Methylation by Transferred Learning Based Neural Network. *J. Comput. Sci. Technol.* **2022**, *37*, 320–329. [CrossRef]
12. Shi, Y.; Shao, S.; Zhang, X.; Wang, Y.; Wu, Y. Error exponent for concatenated codes in DNA data storage under substitution errors. *Sci. China Inf. Sci.* **2022**, *65*, 159304. [CrossRef]
13. Fowler, J.H.; Settle, J.E.; Christakis, N.A. Correlated genotypes in friendship networks. *Proc. Natl. Acad. Sci. USA* **2011**, *108*, 1993–1997. [CrossRef] [PubMed]
14. Humbert, M.; Ayday, E.; Hubaux, J.P.; Telenti, A. Addressing the concerns of the lacks family: Quantification of kin genomic privacy. In Proceedings of the ACM Sigsac Conference on Computer and Communications Security, Berlin, Germany, 4–8 November 2013.
15. DNA Profiles from Ancestry Websites Helped Identify the Golden State Killer Suspect. Available online: https://www.vox.com/2018/4/27/17290288/golden-state-killer-joseph-james-deangelo-dna-profile-match (accessed on 1 January 2018).
16. Greshake, B.; Bayer, P.E.; Rausch, H.; Reda, J. openSNP—A crowdsourced web resource for personal genomics. *PLoS ONE* **2014**, *9*, e89204. [CrossRef] [PubMed]
17. Ball, M.P.; Bobe, J.R.; Chou, M.F.; Clegg, T.; Estep, P.W.; Lunshof, J.E.; Vandewege, W.; Zaranek, A.W.; Church, G.M. Harvard Personal Genome Project: Lessons from participatory public research. *Genome Med.* **2014**, *6*, 10. [CrossRef] [PubMed]
18. Scaraglino, P. Complying with HIPAA: A guide for the university and its counsel. *J. Coll. Univ. Law* **2002**, *29*, 525.
19. GenomePrivacy. Available online: https://genomeprivacy.org/ (accessed on 1 January 2021).
20. Schadt, E.E.; Woo, S.; Hao, K. Bayesian method to predict individual SNP genotypes from gene expression data. *Nat. Genet.* **2012**, *44*, 603–608. [CrossRef]

21. Backes, M.; Berrang, P.; Bieg, M.; Eils, R.; Herrmann, C.; Humbert, M.; Lehmann, I. Identifying personal DNA methylation profiles by genotype inference. In Proceedings of the 2017 IEEE Symposium on Security and Privacy (SP), San Jose, CA, USA, 22–26 May 2017; pp. 957–976.
22. Sero, D.; Zaidi, A.; Li, J.; White, J.D.; Zarzar, T.B.G.; Marazita, M.L.; Weinberg, S.M.; Suetens, P.; Vandermeulen, D.; Wagner, J.K.; et al. Facial recognition from DNA using face-to-DNA classifiers. *Nat. Commun.* **2019**, *10*, 2557. [CrossRef]
23. Lippert, C.; Sabatini, R.; Maher, M.C.; Kang, E.Y.; Lee, S.; Arikan, O.; Harley, A.; Bernal, A.; Garst, P.; Lavrenko, V.; et al. Identification of individuals by trait prediction using whole-genome sequencing data. *Proc. Natl. Acad. Sci. USA* **2017**, *114*, 10166–10171. [CrossRef]
24. Jones, J. An introduction to factor analysis of information risk (fair). *Norwich J. Inf. Assur.* **2006**, *2*, 67.
25. Kim, S.; Misra, A. SNP genotyping: Technologies and biomedical applications. *Annu. Rev. Biomed. Eng.* **2007**, *9*, 289–320. [CrossRef]
26. Johnson, A.D.; O'Donnell, C.J. An Open Access Database of Genome-wide Association Results. *BMC Med. Genet.* **2009**, *10*, 6. [CrossRef]
27. Liu, B.H. *Statistical Genomics: Linkage, Mapping, and QTL Analysis*; CRC Press: Boca Raton, FL, USA, 2017.
28. Reay, W.R.; Atkins, J.R.; Carr, V.J.; Green, M.J.; Cairns, M.J. Pharmacological enrichment of polygenic risk for precision medicine in complex disorders. *Sci. Rep.* **2020**, *10*, 879. [CrossRef] [PubMed]
29. Ng, B.; White, C.C.; Klein, H.U.; Sieberts, S.K.; McCabe, C.; Patrick, E.; Xu, J.; Yu, L.; Gaiteri, C.; Bennett, D.A.; et al. An xQTL map integrates the genetic architecture of the human brain's transcriptome and epigenome. *Nat. Neurosci.* **2017**, *20*, 1418. [CrossRef] [PubMed]
30. Gillespie, J.H. *Population Genetics: A Concise Guide*; JHU Press: Baltimore, MD, USA, 2004.
31. Hernandez, R.D.; Uricchio, L.H.; Hartman, K.; Ye, C.; Dahl, A.; Zaitlen, N. Ultrarare variants drive substantial cis heritability of human gene expression. *Nat. Genet.* **2019**, *51*, 1349–1355. [CrossRef]
32. Yaniv, E.; Arvind, N. Routes for breaching and protecting genetic privacy. *Nat. Rev. Genet.* **2014**, *15*, 409–421.
33. Pakstis, A.J.; Speed, W.C.; Fang, R.; Hyland, F.C.; Furtado, M.R.; Kidd, J.R.; Kidd, K.K. SNPs for a universal individual identification panel. *Hum. Genet.* **2010**, *127*, 315–324. [CrossRef] [PubMed]
34. Lin, Z.; Owen, A.B.; Altman, R.B. Genomic research and human subject privacy. *Science* **2004**, *305*, 183. [CrossRef]
35. Beacon Network. Available online: https://beacon-network.org/ (accessed on 1 January 2018).
36. Shringarpure, S.S.; Bustamante, C.D. Privacy risks from genomic data-sharing beacons. *Am. J. Hum. Genet.* **2015**, *97*, 631–646. [CrossRef]
37. Hagestedt, I.; Zhang, Y.; Humbert, M.; Berrang, P.; Tang, H.; Wang, X.; Backes, M. MBeacon: Privacy-Preserving Beacons for DNA Methylation Data. In Proceedings of the Network and Distributed System Security Symposium, San Diego, CA, USA, 24–27 February 2019.
38. Homer, N.; Szelinger, S.; Redman, M.; Duggan, D.; Tembe, W.; Muehling, J.; Pearson, J.V.; Stephan, D.A.; Nelson, S.F.; Craig, D.W. Resolving individuals contributing trace amounts of DNA to highly complex mixtures using high-density SNP genotyping microarrays. *PLoS Genet.* **2008**, *4*, e1000167. [CrossRef]
39. Jacobs, K.B.; Yeager, M.; Wacholder, S.; Craig, D.; Kraft, P.; Hunter, D.J.; Paschal, J.; Manolio, T.A.; Tucker, M.; Hoover, R.N.; et al. A new statistic and its power to infer membership in a genome-wide association study using genotype frequencies. *Nat. Genet.* **2009**, *41*, 1253–1257. [CrossRef]
40. Visscher, P.M.; Hill, W.G. The limits of individual identification from sample allele frequencies: Theory and statistical analysis. *PLoS Genet.* **2009**, *5*, e1000628. [CrossRef]
41. Sankararaman, S.; Obozinski, G.; Jordan, M.I.; Halperin, E. Genomic privacy and limits of individual detection in a pool. *Nat. Genet.* **2009**, *41*, 965–967. [CrossRef] [PubMed]
42. Philibert, R.A.; Terry, N.; Erwin, C.; Philibert, W.J.; Beach, S.R.; Brody, G.H. Methylation array data can simultaneously identify individuals and convey protected health information: An unrecognized ethical concern. *Clin. Epigenet.* **2014**, *6*, 28. [CrossRef] [PubMed]
43. Dyke, S.O.; Cheung, W.A.; Joly, Y.; Ammerpohl, O.; Lutsik, P.; Rothstein, M.A.; Caron, M.; Busche, S.; Bourque, G.; Rönnblom, L.; et al. Epigenome data release: A participant-centered approach to privacy protection. *Genome Biol.* **2015**, *16*, 142. [CrossRef] [PubMed]
44. Venkatesaramani, R.; Malin, B.A.; Vorobeychik, Y. Re-identification of Individuals in Genomic Datasets Using Public Face Images. *arXiv* **2021**, arXiv:2102.08557.
45. Gymrek, M.; McGuire, A.L.; Golan, D.; Halperin, E.; Erlich, Y. Identifying personal genomes by surname inference. *Science* **2013**, *339*, 321–324. [CrossRef]
46. Backes, M.; Berrang, P.; Humbert, M.; Shen, X.; Wolf, V. Simulating the large-scale erosion of genomic privacy over time. *IEEE/ACM Trans. Comput. Biol. Bioinform.* **2018**, *15*, 1405–1412. [CrossRef]
47. Berrang, P.; Humbert, M.; Zhang, Y.; Lehmann, I.; Eils, R.; Backes, M. Dissecting privacy risks in biomedical data. In Proceedings of the 2018 IEEE European Symposium on Security and Privacy (EuroS&P), London, UK, 24–26 April 2018; pp. 62–76.
48. Sasayama, D.; Hattori, K.; Ogawa, S.; Yokota, Y.; Matsumura, R.; Teraishi, T.; Hori, H.; Ota, M.; Yoshida, S.; Kunugi, H. Genome-wide quantitative trait loci mapping of the human cerebrospinal fluid proteome. *Hum. Mol. Genet.* **2016**, *26*, 44–51. [CrossRef]

49. Humbert, M.; Huguenin, K.; Hugonot, J.; Ayday, E.; Hubaux, J.P. De-anonymizing genomic databases using phenotypic traits. *Proc. Priv. Enhancing Technol.* **2015**, *2015*, 99–114. [CrossRef]
50. Deciphering the Map of RNA Modifications from Epitranscriptome Sequencing Data. Available online: https://rna.sysu.edu.cn/rmbase/ (accessed on 1 January 2018).
51. dbSNP. Available online: https://www.ncbi.nlm.nih.gov/SNP/ (accessed on 1 January 2018).
52. Ramos, E.M.; Din-Lovinescu, C.; Bookman, E.B.; McNeil, L.J.; Baker, C.C.; Godynskiy, G.; Harris, E.L.; Lehner, T.; McKeon, C.; Moss, J.; et al. A mechanism for controlled access to GWAS data: Experience of the GAIN Data Access Committee. *Am. J. Hum. Genet.* **2013**, *92*, 479–488.

[CrossRef]

53. He, M.; Zou, D.; Qiang, W.; Wu, W.; Xu, S.; Deng, X.; Jin, H. Utility-Prioritized Differential Privacy for Quantitative Biomedical Data. *J. Circuits, Syst. Comput.* **2022**, *31*, 2250236. [CrossRef]
54. Fienberg, S.E.; Slavkovic, A.; Uhler, C. Privacy preserving GWAS data sharing. In Proceedings of the 2011 IEEE 11th International Conference on Data Mining Workshops, Vancouver, BC, Canada, 11 December 2011; pp. 628–635.